Wind and Structures, *Vol. 21, No. 6 (2015) 727-753*
DOI: http://dx.doi.org/10.12989/was.2015.21.6.727

Design feasibility of double-skinned composite tubular wind turbine tower

Taek Hee Han[1a], Young Hyun Park[1b], Deokhee Won[2c] and Joo-Ha Lee[*3]

[1]*Coastal Development Research Center, Korea Institute of Ocean Science and Technology, 787 Haeanro, Ansan 15627, Korea*
[2]*Coastal Disaster Prevention Research Center, Korea Institute of Ocean Science and Technology, 787 Haeanro, Ansan 15627, Korea*
[3]*Department of Civil Engineering, The University of Suwon, 17 Wauan-gil, Hwaseong, 18323, Korea*

(Received October 11, 2015, Revised November 30, 2015, Accepted December 1, 2015)

Abstract. A double-skinned composite tubular (DSCT) wind power tower was suggested and automatic section design software was developed. The developed software adopted the nonlinear material model and the nonlinear column model. If the outer diameter, material properties and design capacities of a DSCT wind power tower are given, the developed software performs axial force-bending moment interaction analyses for hundreds of sections of the tower and suggests ten optimized cross-sectional designs. In this study, 80 sections of DSCT wind power towers were designed for 3.6 MW and 5.0 MW turbines. Moreover, the performances of the 80 designed sections were analyzed with and without considerations of large displacement effect. In designing and analyzing them, the material nonlinearity and the confining effect of concrete were considered. The comparison of the analysis results showed the moment capacity loss of the wind power tower by the mass of the turbine is significant and the large displacement effect should be considered for the safe design of the wind power tower.

Keywords: wind tower; column; DSCT; composite; large displacement effect

1. Introduction

Due to high energy prices and supply uncertainties, many countries are trying to develop renewable energies such as wind power, tidal power, geothermal power and photovoltaic power. Among them, wind power is considered as providing the best energy efficiency. Several offshore wind farms are have been planned and constructed over the world. According to GWEC (Global Wind Energy Council), the size of the installed wind turbines had reached to 282,430 MW in the world until 2012. The world average annual growth rate of wind turbine installation from 1996 to 2012 was 27.7% and the annual growth rate in the year of 2012 was 18.7%. Owing to the growth of offshore wind energy market, in 2009, the size of wind turbine installation has grown from

*Corresponding author, Assistant professor, E-mail: leejooha@suwon.ac.kr
[a] Ph.D., E-mail: taekheehan@kiost.ac.kr
[b] Ph.D., E-mail: yhpark@kiost.ac.kr
[c] Ph.D., E-mail: thekeyone@kiost.ac.kr

http://www.techno-press.org/?journal=was&subpage=8 ISSN: 1226-6116 (Print), 1598-6225 (Online)

26,721 MW to 38,708 MW by 44.8% (Sawyer 2013).

The offshore wind power industry started to grow from the 1980's due to companies and government focusing on the development of offshore wind farms. In 2008, the offshore wind farms generated 25,413TWh/year. In this time, United Kingdom and several countries in Europe were leading the offshore wind farm construction and operation. Table 1 shows the installed capacity of offshore farm and Table 2 shows the offshore wind farm development plan of South Korea (Sung 2012).

Because of better wind quality on offshore than onshore, the number of offshore wind farm has increases. To build an economic wind farm, it is important to select a suitable wind farm site (Unchai and Janyalertadun 2014) and to evaluate the wind energy (Chen and Tran 2015). Also the arrangement (Choi *et al*. 2015) and safety of the wind power towers. Moreover, the generating turbines, blades, and towers are getting bigger and taller. However, as the tower becomes taller, its slenderness ratio increases. This large slenderness ratio makes a tower easy to buckle or to fail as shown in Fig. 1.

Table 1 Top 10 EU Countries in Offshore Wind Power (Sawyer 2013)

Country	No. of farms	No. of turbines	Capacity installed (MW)
UK	20	870	2,947.9
Denmark	12	416	921.0
Belgium	2	91	379.5
Germany	6	68	280.3
Netherlands	4	124	246.8
Sweden	6	75	163.7
Finland	2	9	26.3
Ireland	1	7	25.2
Norway	1	1	2.3
Portugal	1	1	2.0
Total	55	1,662	4,995

Table 2 Offshore Wind Farm Development Plan of Korea (Sung 2012)

Plant	Capacity (MW)	Remark
Southwest Sea	2,500	Investigating wind condition
Jeonnam	4,000	Investigating wind condition
Sam-Mu	30	'12.7 (constructing)
Daejeong	200	Design process
Han-Lim	150	Investigating wind condition
Haengwon	60	Design process
Total	6,940	

Therefore, to reduce the failure possibility of a tall tower, a new-type tower structure, which has high strength, is required. In this study, a double-skinned concrete filled tube (DSCT) was adopted as the wind tower to enhance its load-resisting capacity. Additionally, automatic section design software of a DSCT wind power tower was developed based on the nonlinear material model (Han *et al.* 2010) and the nonlinear column model (Han *et al.* 2013) considering the confining effect of concrete. By using the developed software, the sections of the DSCT wind power towers were designed and their moment resisting capacities were evaluated. The designed sections of DSCT towers were set to satisfy the required capacities to support 3.6 MW and 5.0 MW turbines, which were supported by the reference steel wind power towers.

2. Automatıc desıgn program for DSCT tower

2.1 Basic theory of DCST column

A DSCT column was introduced by Shakir-Khalil and Illouli in 1987. It is a column which is composed of two concentric tubes and concrete between the two tubes as shown in Fig. 2. After their introduction, the axial strength of the DSCT column was studied (Wei *et al*. 1995, Zhao and Grzebieta 2002, Tao *et al*. 2004) and it was reported that the axial strength of a DSCT column was higher than the sum of axial strengths from the inner tube, outer tube, and concrete (Wei *et al.* 1995). Furthermore, a hybrid DSCT column, which is composed of fiber reinforced polymer (FRP) tubes and concrete, has been studied (Teng *et al.* 2006, Yu *et al.* 2006). Recently, Han *et al.* (2010, 2013) proposed the material nonlinear model and column model of a DSCT column and studied the bending strength of a DSCT column.

Fig. 1 Failure of steel wind tower (Khatri 2013; http://galleryhip.com; Ruralgrubby's Wind Watch)

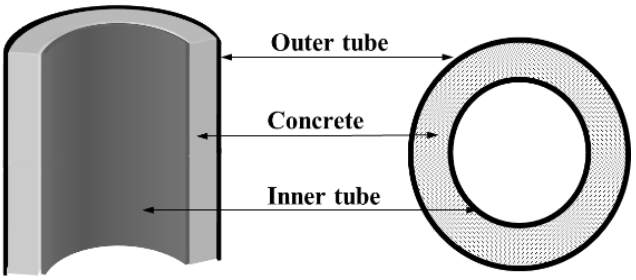

Fig. 2 Cross section of DSCT column

In this study, an automatic section design program for a DSCT tower was coded with FORTRAN language. It is based on the nonlinear model of a DSCT column (Han *et al.* 2013). The strain compatibility of a DSCT tower is derived from the section analysis as shown in Fig. 3, and the relation of curvature and lateral displacement is defined from Fig. 4. The column model uses a section analysis and adopted the layer-by-layer technique for numerical integration of stresses (Kilpatrick and Ranagan 1997). The stresses in the layers of the concrete and the tubes are calculated as the change of strain. Axial loads and moments for the concrete and the tubes are given as Eqs. (1)-(8) (Han *et al.* 2013).

$$P_i^{CC} = \sum_{j=1}^{n} P_{i,j}^{CC} = \sum_{j=1}^{n} A_{i,j}^{CC} \cdot f_{i,j}^{CC} \tag{1}$$

$$P_i^{IT} = \sum_{j=1}^{n} P_{i,j}^{IT} = \sum_{j=1}^{n} A_{i,j}^{IT} \cdot f_{i,j}^{IT} \tag{2}$$

$$P_i^{OT} = \sum_{j=1}^{n} P_{i,j}^{OT} = \sum_{j=1}^{n} A_{i,j}^{OT} \cdot f_{i,j}^{OT} \tag{3}$$

$$M_i^{CC} = \sum_{j=1}^{n} M_{i,j}^{CC} = \sum_{j=1}^{n} P_{i,j}^{CC} \cdot x_{i,j}^{CC} \tag{4}$$

$$M_i^{IT} = \sum_{j=1}^{n} M_{i,j}^{IT} = \sum_{j=1}^{n} P_{i,j}^{IT} \cdot x_{i,j}^{IT} \tag{5}$$

$$M_i^{OT} = \sum_{j=1}^{n} M_{i,j}^{OT} = \sum_{j=1}^{n} P_{i,j}^{OT} \cdot x_{i,j}^{OT} \tag{6}$$

$$P_i = P_i^{CC} + P_i^{IT} + P_i^{OT} \tag{7}$$

$$M_i = M_i^{CC} + M_i^{IT} + M_i^{OT} \tag{8}$$

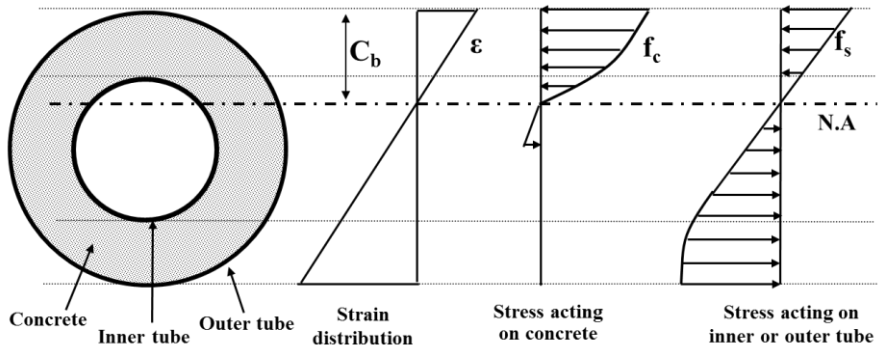

Fig. 3 Section analysis using strain compatibility and layer-by-layer approach (Han *et al.* 2013)

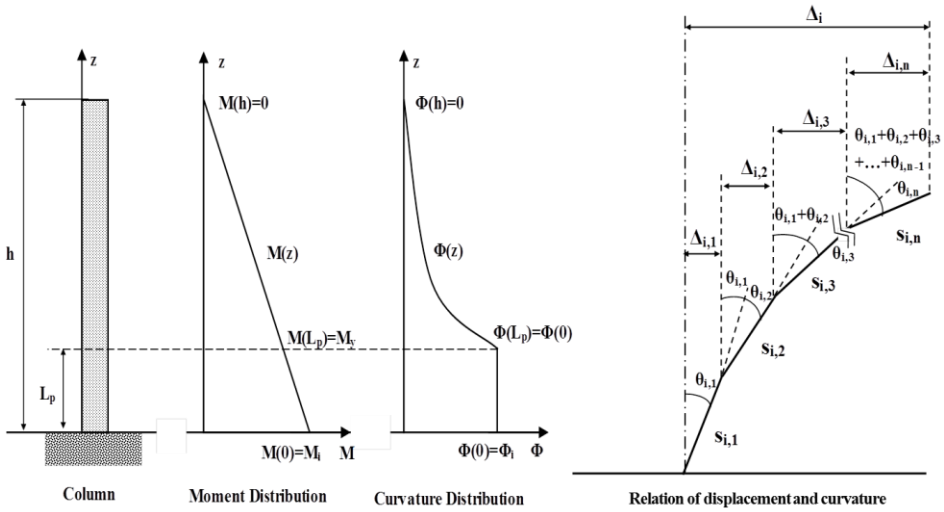

Fig. 4 Curvature and displacement functions (Han *et al.* 2013)

If a column is divided into numerous small elements along its height, the curvature corresponding to the each element can be calculated from the curvature function (Han *et al.* 2013). Fig. 4 shows the column composed of a certain numbers of elements which have the length of $S_{i,j}$. The rotation angle is given as Eq. (9) from the curvature function. The lateral displacement of the top point of the column can be calculated by summating the lateral displacements of all elements in the stage of the strain distribution as Eq. (10) (Han *et al.* 2013).

$$\theta_{i,j} = \varphi(z) \cdot S_{i,j} \tag{9}$$

$$\Delta_i = \sum_{j=1}^{n} \Delta_{i,j} = \sum_{j=1}^{n} \left(S_{i,j} \sum_{k=1}^{j} \theta_{i,k} \right) \tag{10}$$

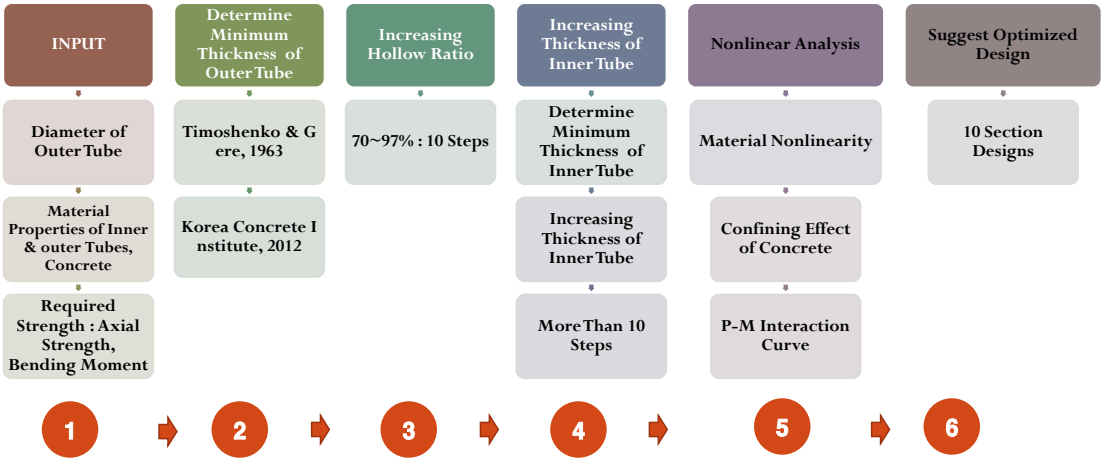

Fig. 5 Design process in developed programs

2.2 Automatic design program

The developed design program, Auto DSCT® (Han 2014), performs the section design of a DSCT tower by the procedure as shown in Fig. 5. It performs axial load-bending moment (P-M) interaction and lateral force-lateral displacement (P-Δ) analysis when it is given the input data which contains the information of outer diameter, the material properties, the required bending moment and axial strength of a DSCT tower. During the analysis, it considers the variation of the hollow ratio, the thicknesses of the inner tube, and the thicknesses of the outer tube. As the results, it suggests ten optimum design sections that have satisfied the required capacities. When the outer diameter of a DSCT tower is given, firstly, the program calculates minimum thickness of the outer tube which satisfies Eq. (11) (Timoshenko and Gere 1936) and Eq. (12) (Korea Concrete Institute 2012) to avoid the local buckling failure of a DSCT tower. Eq. (11) is a criterion for the local buckling failure of a cylindrical tube. Eq. (12) is a criterion for the local buckling failure of the steel tube of a circular CFT column. Moreover it determines the calculated outer tube thickness as the most economic thickness.

$$f_{cr} = \frac{t \cdot E}{\frac{D}{2}\sqrt{3(1-v^2)}} \tag{11}$$

$$t > (D+t)\sqrt{\frac{f_y}{8E}} \tag{12}$$

$$t_i > \frac{D_i \cdot f_y \cdot t}{D \cdot f_{iy}} \tag{13}$$

$$t_i = \sqrt{\frac{6D_i^2 \cdot f_y \cdot t}{2.27D \cdot E_i}} \tag{14}$$

After determination of the thickness of the outer tube, the program varies the hollow ratio of the DSCT tower from 97% to 70% by the step of 3%. The outer diameter of the inner tube is determined by the hollow ratio. The thickness of the inner tube is calculated to satisfy Eqs. (13) and (14) simultaneously (Han *et al.* 2010). After determination of the geometric properties of the DSCT tower, the program performs P-M interaction analysis with increasing the thickness of the inner tube by 0.01mm for the determined ten hollow ratios. The design procedure is as shown in Fig. 5. The P-M interaction analysis, which considers the material nonlinearity and the confining effect of concrete, is performed as the flowchart in Fig. 6. The proposed ten optimum design sections have the thinnest tubes among the given hollow ratio. Because the ten design sections have different hollow ratio, their axial strength and bending strength are different. Therefore, engineers can select one which is proper to their design purpose.

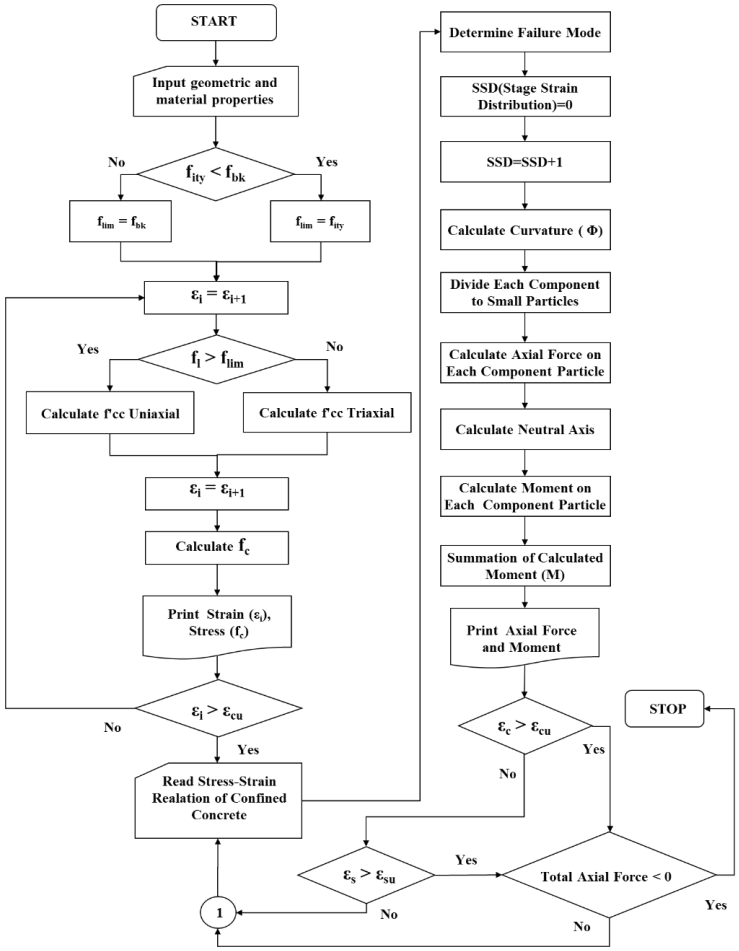

Fig. 6 Flowchart of P-M interaction analysis

3. Design of DSCT wind power tower

3.1 Design load and referece tower

In this study, the design of the steel wind power towers, which were built in Kriegers Flak Offshore Wind Farm (Ljjj and Gravesen 2008) as shown in Fig. 7, was referred to perform automatic design of DSCT wind power towers. 3.6 MW and 5.0 MW turbines were installed in Kriegers Flak Offshore Wind Farm and the dimensions of reference steel towers are summarized in Table 3. As shown in Table 3, the bottom diameters and wall thicknesses of the steel towers are 4.5 m and 30 mm for the 3.6MW turbine; 6.0 m and 35 mm for the 5.0 MW turbine, respectively.

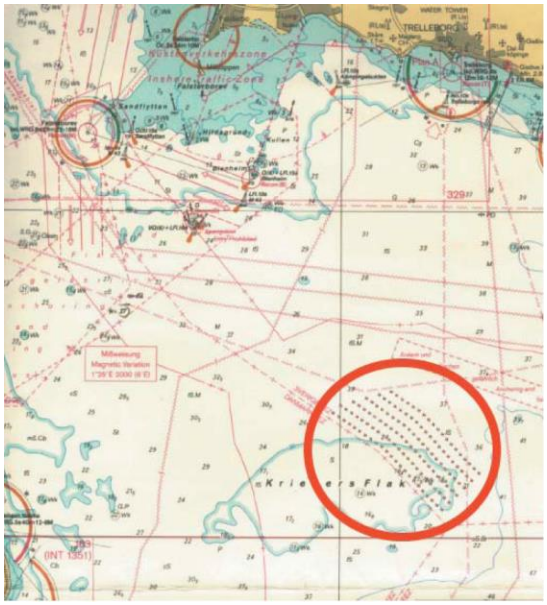

Fig. 7 Map of the western Baltic Sea south of Sweden and the site (Ljjj and Gravesen 2008)

Table 3 Dimension of reference steel tower (Ljjj and Gravesen 2008)

Turbine size	3.6 MW	5 MW
Output power	3.6 MW	5.0 MW
Rotor diameter	106 m	126 m
Foundation–tower interface level acc. MSL*	3.5 m	3.5 m
Hub height above foundation interface	72.5 m	82.5 m
Nacelle mass incl. Rotor	220 tons	410 tons
Tower top diameter/wall thickness	3.5 m/15 mm	4.5 m/20 mm
Tower bottom diameter/wall thickness	4.5 m/30 mm	6.0 m/35 mm
Tower mass	220 tons	300 tons

*MSL: Mean Sea Level

Table 4 Turbine loads (Ljjj and Gravesen 2008)

Turbine design load		Vertical load (MN)	Extreme load		Operational load		Fatigue load m=(4-5) N:1×10^7	
Capacity	Level		F_{ex}	M_{ex}	F_{op}	M_{op}	F_{eq}	M_{eq}
3.6 MW	15 m	4.40	1.42 MN	89.90 MN-m	0.85 MN	54.0 MN-m	0.35 MN	19.20 MN-m
5.0 MW	15 m	7.10	2.03 MN	150.00 MN-m	1.20 MN	90.0 MN-m	0.49 MN	28.10 MN-m

Table 4 shows design vertical loads, extreme loads, operational loads, and fatigue loads which were applied to the steel towers supporting 3.6 MW and 5.0 MW turbines. To design DSCT wind power towers, the largest values of vertical load and extreme bending moment (M_{ex}) Table 4 were selected and they were applied as the required axial strength and bending strength. The automatic design was performed. The DSCT towers were set to have smaller diameters than steel towers and to satisfy the design loads which applied to the steel towers.

3.2 Automatic design of DSCT tower

Automatic design processes were performed for the DSCT towers. The required axial strength and bending strength were 4.40 MN and 89.9 MN-m for 3.6 MW turbine and 7.10 MN and 150.00 MN-m for 5.0 MW turbine, respectively. The DSCT towers were set to have smaller diameters than the reference steel towers. The design case of DSCT tower had 8 different diameters, which were 95%, 80%, 65%, and 50% of diameters of the reference steel towers for 3.6 MW and 5.0 MW turbines. Table 5 shows the design cases of DSCT towers. In the design of DSCT towers, the applied material properties are as follows. The strength of concrete was 29.43 MPa. The yield strength and ultimate strength of the steel tube were 313.60 MPa and 490.50 MPa, respectively.

Table 5 Design case of DSCT tower

Turbine size	Diameter ratio*	Diameter	Design case**
3.6 MW DSCT tower	0.95	4,275 mm	3S95
	0.90	4,050 mm	3S90
	0.85	3,825 mm	3S85
	0.80	3,600 mm	3S80
5.0 MW DSCT tower	0.95	5,700 mm	5S95
	0.90	5,400 mm	5S90
	0.85	5,100 mm	5S85
	0.80	4,800 mm	5S80

*Diameter Ratio: Diameter of DSCT Wind Tower / Diameter of Steel Wind Tower

**Design Case: tSd (e.g., 3S95, 5S80), t=turbine capacity, S=steel tube, d=diameter ratio($\times 10^{-2}$)

Table 6 Designed sections of DSCT wind tower for 3.6 MW turbine

Design Case for 3S95	3S95/97	3S95/94	3S95/91	3S95/88	3S95/85	3S95/82	3S95/79	3S95/76	3S95/73	3S95/70
D (mm)	4275.0	4275.0	4275.0	4275.0	4275.0	4275.0	4275.0	4275.0	4275.0	4275.0
D_i (mm)	4146.8	4018.5	3890.3	3762.0	3633.8	3505.5	3377.3	3249.0	3120.8	2992.5
D_i/D	0.97	0.94	0.91	0.88	0.85	0.82	0.79	0.76	0.73	0.70
t (mm)	5.50	5.50	5.50	5.50	5.50	5.50	5.50	5.50	5.50	5.50
t_i (mm)	10.38	10.06	9.74	9.42	9.09	8.77	8.45	8.13	7.81	7.49
Design Case for 3S90	3S90/97	3S90/94	3S90/91	3S90/88	3S90/85	3S90/82	3S90/79	3S90/76	3S90/73	3S90/70
D (mm)	4050.0	4050.0	4050.0	4050.0	4050.0	4050.0	4050.0	4050.0	4050.0	4050.0
D_i (mm)	3928.5	3807.0	3685.5	3564.0	3442.5	3321.0	3199.5	3078.0	2956.5	2835.0
D_i/D	0.97	0.94	0.91	0.88	0.85	0.82	0.79	0.76	0.73	0.70
t (mm)	5.50	5.50	5.50	5.50	5.50	5.50	6.00	6.00	6.50	6.50
t_i (mm)	10.10	9.79	9.48	9.16	8.85	8.54	8.59	8.27	8.26	7.93
Design Case for 3S85	3S85/97	3S85/94	3S85/91	3S85/88	3S85/85	3S85/82	3S85/79	3S85/76	3S85/73	3S85/70
D (mm)	3825.0	3825.0	3825.0	3825.0	3825.0	3825.0	3825.0	3825.0	3825.0	3825.0
D_i (mm)	3710.3	3595.5	3480.8	3366.0	3251.3	3136.5	3021.8	2907.0	2792.3	2677.5
D_i/D	0.97	0.94	0.91	0.88	0.85	0.82	0.79	0.76	0.73	0.70
t (mm)	6.50	6.00	6.00	6.00	6.50	6.50	7.00	7.50	7.50	8.00
t_i (mm)	10.67	9.94	9.62	9.30	9.35	9.02	9.02	8.98	8.63	8.54
Design Case for 3S80	3S80/97	3S80/94	3S80/91	3S80/88	3S80/85	3S80/82	3S80/79	3S80/76	3S80/73	3S80/70
D (mm)	3600.0	3600.0	3600.0	3600.0	3600.0	3600.0	3600.0	3600.0	3600.0	3600.0
D_i (mm)	3492.0	3384.0	3276.0	3168.0	3060.0	2952.0	2844.0	2736.0	2628.0	2520.0
D_i/D	0.97	0.94	0.91	0.88	0.85	0.82	0.79	0.76	0.73	0.70
t (mm)	8.00	7.50	7.50	7.50	8.00	8.00	8.50	8.50	9.00	9.50
t_i (mm)	11.49	10.78	10.43	10.09	10.07	9.71	9.64	9.28	9.17	9.03

The designed sections of DSCT towers, which were recommended by the developed program are summarized in Tables 6 and 7, for the 3.6 MW and 5.0 MW turbines, respectively. In the tables, the number following after the design case (such as /97, /94, and so on) represents the hollow ratio of the designed DSCT tower. Therefore, the design case 3S95/88 represents a DSCT tower which has an outer tube with 95% diameter of steel tower for the 3.6 MW turbine and the hollow ratio of 0.88. The design case of 5S85/91 means a DSCT tower which has an outer tube with 85% diameter of steel tower for the 5.0 MW turbine and the hollow ratio of 0.91. The recommended design cases are the most economic sections at the each hollow ratio (D_i/D) because they have the

smallest thicknesses of the inner and outer tubes. When the hollow ratio decreases, the thicknesses of the inner and outer tubes decrease. This means that a DSCT tower with a smaller hollow ratio requires much concrete but less steel.

Figs. 8 and 9 show P-M interaction curves of the designed DSCT towers. They shows that all the designed sections satisfy the required axial strengths and bending strengths. Because the bending moment governs the behavior of a wind power tower, all the designed DSCT towers have excessive axial strengths. As the hollow decreases, the axial and bending strengths of the DSCT tower increase because the smaller hollow ratio makes a DSCT tower to have thicker concrete wall. In the general, a DSCT tower with larger hollow ratio is economic although it has the thicker inner tube.

Table 7 Designed sections of DSCT wind tower for 5.0 MW turbine

Design Case for 5S95	5S95/97	5S95/94	5S95/91	5S95/88	5S95/85	5S95/82	5S95/79	5S95/76	5S95/73	5S95/70
D (mm)	5700.0	5700.0	5700.0	5700.0	5700.0	5700.0	5700.0	5700.0	5700.0	5700.0
D_i (mm)	5529.0	5358.0	5187.0	5016.0	4845.0	4674.0	4503.0	4332.0	4161.0	3990.0
D_i / D	0.97	0.94	0.91	0.88	0.85	0.82	0.79	0.76	0.73	0.70
t (mm)	7.50	7.50	7.50	7.50	7.50	7.50	7.50	7.50	7.50	7.50
t_i (mm)	13.99	13.56	13.13	12.70	12.26	11.83	11.40	10.96	10.53	10.10
Design Case for 5S90	5S90/97	5S90/94	5S90/91	5S90/88	5S90/85	5S90/82	5S90/79	5S90/76	5S90/73	5S90/70
D (mm)	5400.0	5400.0	5400.0	5400.0	5400.0	5400.0	5400.0	5400.0	5400.0	5400.0
D_i (mm)	5238.0	5076.0	4914.0	4752.0	4590.0	4428.0	4266.0	4104.0	3942.0	3780.0
D_i / D	0.97	0.94	0.91	0.88	0.85	0.82	0.79	0.76	0.73	0.70
t (mm)	7.00	7.00	7.00	7.00	7.00	7.00	7.00	7.00	7.00	7.00
t_i (mm)	13.16	12.75	12.35	11.94	11.53	11.12	10.72	10.31	9.90	9.50
Design Case for 5S85	5S85/97	5S85/94	5S85/91	5S85/88	5S85/85	5S85/82	5S85/79	5S85/76	5S85/73	5S85/70
D (mm)	5100.0	5100.0	5100.0	5100.0	5100.0	5100.0	5100.0	5100.0	5100.0	5100.0
D_i (mm)	4947.0	4794.0	4641.0	4488.0	4335.0	4182.0	4029.0	3876.0	3723.0	3570.0
D_i / D	0.97	0.94	0.91	0.88	0.85	0.82	0.79	0.76	0.73	0.70
t (mm)	6.50	6.50	6.50	6.50	6.50	6.50	6.50	6.50	6.50	6.50
t_i (mm)	12.32	11.94	11.56	11.18	10.80	10.42	10.04	9.66	9.27	8.89
Design Case for 5S80	5S80/97	5S80/94	5S80/91	5S80/88	5S80/85	5S80/82	5S80/79	5S80/76	5S80/73	5S80/70
D (mm)	4800.0	4800.0	4800.0	4800.0	4800.0	4800.0	4800.0	4800.0	4800.0	4800.0
D_i (mm)	4656.0	4512.0	4368.0	4224.0	4080.0	3936.0	3792.0	3648.0	3504.0	3360.0
D_i / D	0.97	0.94	0.91	0.88	0.85	0.82	0.79	0.76	0.73	0.70
t (mm)	6.50	6.50	6.50	6.50	6.50	6.50	7.00	7.00	7.50	8.00
t_i (mm)	11.96	11.59	11.22	10.85	10.48	10.11	10.10	9.72	9.66	9.57

Figs. 8(d) and 9(d) show the DSCT towers have sufficient strengths to support a 3.6 MW turbine and 5.0 MW turbine, respectively, although their outer diameters are much smaller than those of the reference steel towers. The axial load of the criterion is the sum of the installed turbine weight and the self-weight of reference steel tower.

4. Lateral behavior analysis considering large displacement effect

4.1 Large displacement effect

The behavior of a wind power tower is mainly governed by the lateral load which results from wind. However, the axial load by the mass of turbine is not negligible but significant. As shown in Table 3, the total mass of the 3.6 MW nacelle and its blades is 220 ton. And 5.0 MW turbine nacelle including blades weighs 410 ton. Considering the mass of a turbine, a wind power tower is a very slender structure.

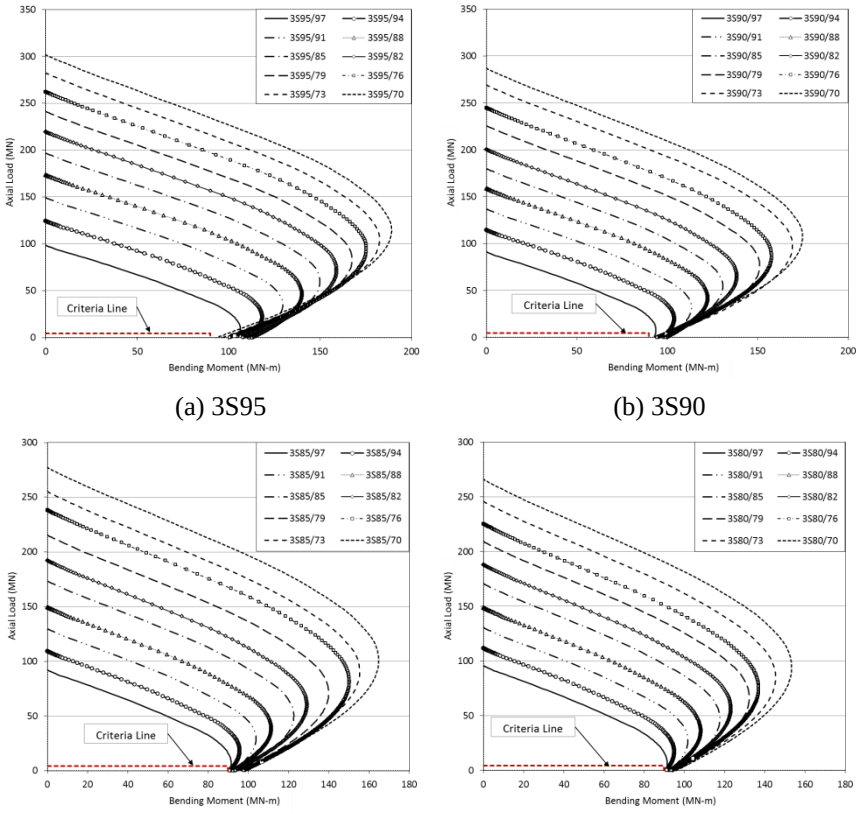

(a) 3S95 (b) 3S90

(c) 3S85 (d) 3S80

Fig. 8 P-M interaction curves of designed DSCT wind towers for 3.6 MW turbine

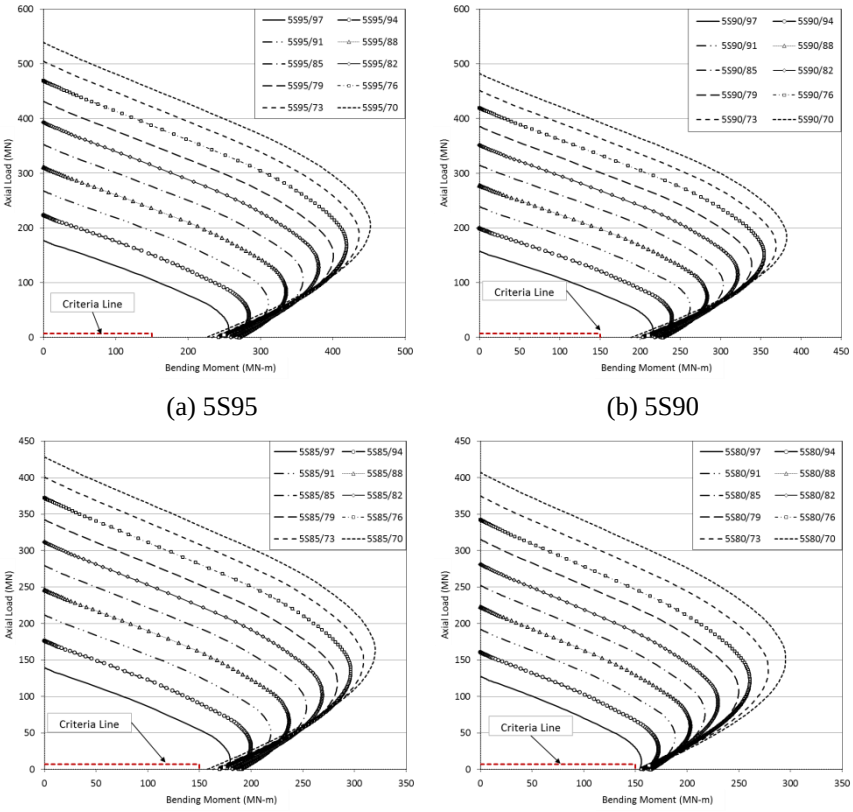

(a) 5S95 (b) 5S90

(c) 5S85 (d) 5S80

Fig. 9 P-M interaction curves of designed DSCT wind towers for 5.0 MW turbine

The mass of a wind turbine which is located on the top of a slender wind tower makes additional moment by gravity as the wind tower is bent by the lateral force such the wind load. In this case, the lateral displacement is the moment arm of the vertical force by the turbine mass and gravity as shown in Fig. 10. This additional moment makes the tower cannot exert its original moment resisting capacity against the lateral force. Therefore, for the safe design of a wind tower, this additional moment effect by the mass on the top of the tower, which is large displacement effect (LDE), should be considered and evaluated. The hub heights above foundation interface are 72.5 m and 82.5 m for the 3.6 MW and 5.0 MW turbines, respectively.

As shown in Fig. 10, the moment resisting capacity (nominal bending strength, M_n) can be decomposed into the moment resisting lateral load (M_L) and the moment induced by the mass of a turbine (M_W). The moment resisting capacity (M_n) is defined by the design of the tower section. The moment induced by the weight of a turbine (M_W) increases in proportion to the amount of the lateral displacement of the tower. The moment resisting capacity to the lateral loads (M_L) is smaller than the nominal bending strength (M_n) if the large displacement effect is considered. Therefore, it is rational that the moment resisting lateral load (M_L) is evaluated as the actual moment resisting capacity. It can be summarized by Eq. (15)-(17). Where, h_T is the height from the top of the footing to the center of the hub and Δ_N is the lateral displacement of the center of gravity of the turbine.

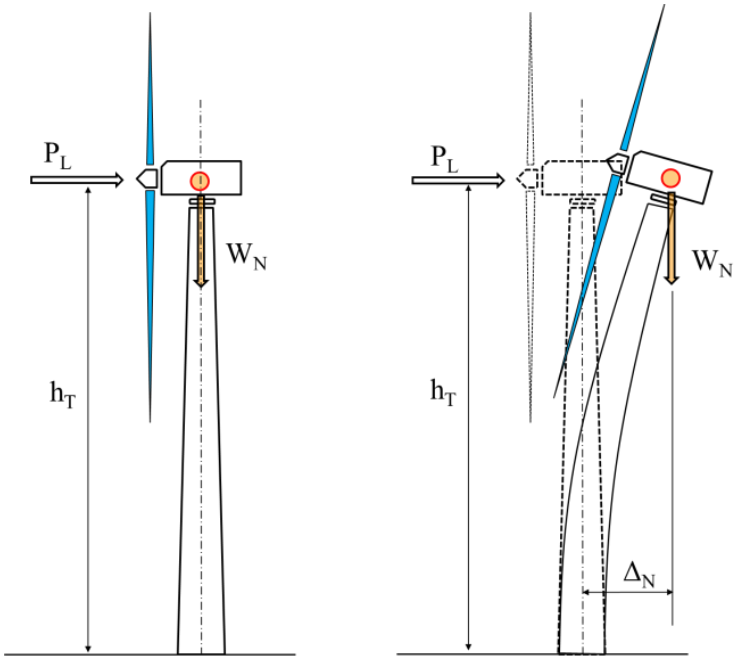

Fig. 10 Consideration of large displacement effect

$$M_n = M_L + M_W \tag{15}$$

$$M_L = P_L \times h_T \tag{16}$$

$$M_W = W_N \times \Delta_N \tag{17}$$

4.2 Lateral behavior analysis

The moment-displacement relation analyses were performed for the 80 designed DSCT wind towers by CoWiTA® (Han 2015). In the analyses, the material nonlinearities of concrete and steel were considered. Moreover, the confining effect of concrete was considered. CoWiTA® use Mander *et al.*'s unified concrete model (1988) as the concrete model. Figs. 11 and 12 show the applied concrete model and the steel model in CoWiTA®, respectively.

The 80 designed towers were analyzed with and without consideration of large displacement (LDE and SDE) and their results were compared. In the analyses, 4.4 MN and 7.1 MN were applied as the vertical loads by the 3.6MW turbine and the 5.0 MW turbine, respectively. Because these values include the weight of the tower, the actual vertical loads are smaller than them. But these values were applied for conservative designs.

Figs. 13-16 show the analysis results and comparison when large displacement effect was considered (LDE) and not considered (SDE). Fig. 13 shows the lateral load-lateral displacement

relation of DSCT towers for 3.6MW turbines without consideration of large displacement effect (SDE). In this case, the lateral load increases as the displacement increases. In the case of 3S95 (SDE), all the designed DSCT towers satisfy the required bending moment capacity (=89.90MN-m). In the cases of 3S90 (SDE), 3S85 (SDE), and 3S90 (SDE), most of deigned DSCT towers satisfy the required bending moment capacity except some DSCT towers with large hollow ratios. The bending moment resisting capacities in Fig. 13 are equal to the nominal bending strengths (M_n) which is calculated by Eq. (15).

Fig. 14 shows the lateral load-lateral displacement relation of DSCT towers for 3.6 MW turbines with consideration of large displacement effect (LDE). In this case, the lateral load increases to the peak point and decreases after the peak point as displacement increase. When Fig. 14 is compared with Fig. 13, it is observed that the bending moment strengths decrease and by large displacement effect.

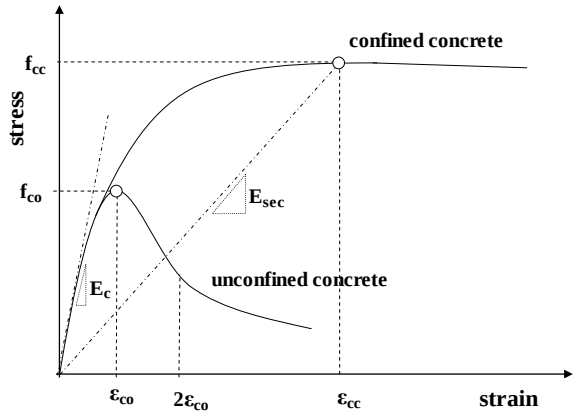

Fig. 11 Applied concrete model (Mander et al. 1988)

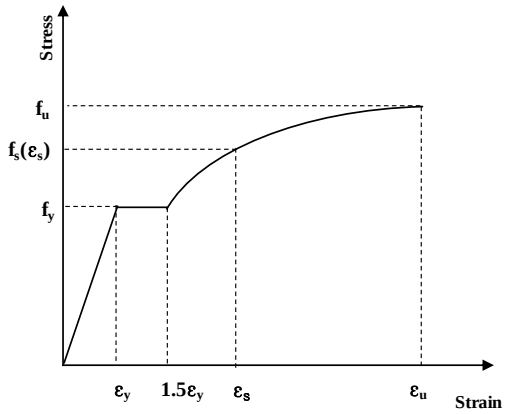

Fig. 12 Applied steel model (Han *et al.* 2013)

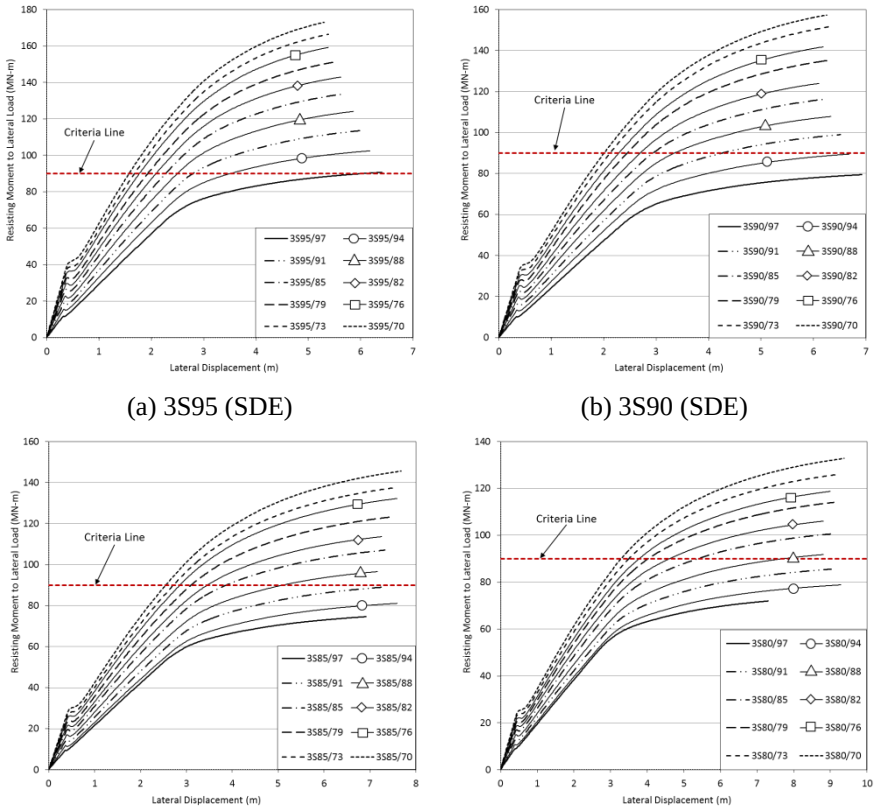

(a) 3S95 (SDE) (b) 3S90 (SDE)

(c) 3S85 (SDE) (d) 3S80 (SDE)

Fig. 13 Moment resisting capacity of designed DSCT towers for 3.6 MW (SDE)

Some design cases which were evaluated to be safe when large displacement effect was not considered such as 3S95/94, 3S90/88, 3S85/82, and 3S80/73 are judged not to be safe. Moreover, most of the design case of 3S80 does not satisfy the required bending moment capacity. Therefore, it is very important to consider large displacement effect for a safe design of a slender beam-column structure such as a wind power tower. The bending moment resisting capacities in Fig. 14 are equal to the moment resisting lateral load (M_L) which is calculated by Eq. (16). The analysis results such as peak moment, dissipated energy, and energy ductility ratio of the designed DSCT towers for 3.6 MW turbines are summarized in Table 8.

Fig. 15 shows the lateral load-lateral displacement relation of DSCT towers for 5.0 MW turbines without consideration of large displacement effect (SDE). In this case, the lateral load increases as the displacement increases. All the designed DSCT towers satisfy the required bending moment capacity (=150.00 MN-m) except 5S80/97 which have the smallest diameter and the largest hollow ratio in the design cases. The bending moment resisting capacities in Fig. 15 are equal to the nominal bending strengths (M_n) which is calculated by Eq. (15).

Table 8 Analysis result of DSCT wind tower for 3.6 MW turbine

Design case	Hollow ratio (%)	Peak moment (MN-m)			Displacement at peak moment (m)			Dissipated energy (MN-m)			Energy ductility ratio		
		SDE	LDE	LDE /SDE	SDE	LDE	LDE /SDE	SDE	LDE	LDE /SDE	SDE	LDE	LDE /SDE
3S80	70	132.78	94.60	0.71	9.36	7.03	0.75	12.26	9.67	0.79	2.44	3.53	1.45
	73	125.94	88.84	0.71	9.17	6.84	0.75	11.39	8.90	0.78	2.46	3.54	1.44
	76	118.74	82.77	0.70	8.98	6.54	0.73	10.52	8.13	0.77	2.48	3.55	1.43
	79	114.03	78.40	0.69	9.08	6.34	0.70	10.26	7.82	0.76	2.56	3.69	1.44
	82	106.04	71.94	0.68	8.79	6.00	0.68	9.24	6.94	0.75	2.60	3.69	1.42
	85	100.57	66.85	0.66	8.98	5.75	0.64	9.02	6.62	0.73	2.73	3.88	1.42
	88	91.80	59.66	0.65	8.79	5.38	0.61	8.08	5.78	0.71	2.81	3.95	1.41
	91	85.54	54.27	0.63	9.00	5.05	0.56	7.80	5.37	0.69	3.03	4.20	1.39
	94	78.85	48.79	0.62	9.26	4.41	0.48	7.51	4.93	0.66	3.29	4.32	1.31
	97	74.59	45.82	0.61	9.84	4.00	0.41	7.74	4.80	0.62	3.79	4.08	1.08
3S85	70	145.57	112.57	0.77	7.66	6.75	0.88	10.79	9.07	0.84	2.24	2.94	1.31
	73	137.37	105.26	0.77	7.48	6.55	0.87	9.93	8.29	0.83	2.25	2.93	1.31
	76	132.21	100.05	0.76	7.57	6.41	0.85	9.70	8.02	0.83	2.31	3.03	1.31
	79	123.13	91.91	0.75	7.41	6.15	0.83	8.83	7.23	0.82	2.31	3.06	1.33
	82	113.62	83.45	0.73	7.24	5.84	0.81	7.95	6.42	0.81	2.33	3.08	1.32
	85	107.04	77.16	0.72	7.31	5.62	0.77	7.60	6.04	0.79	2.42	3.23	1.33
	88	96.58	67.95	0.70	7.15	5.25	0.73	6.71	5.21	0.78	2.47	3.28	1.33
	91	89.09	60.88	0.68	7.32	4.96	0.68	6.41	4.83	0.75	2.61	3.50	1.34
	94	81.09	53.60	0.66	7.57	4.61	0.61	6.12	4.41	0.72	2.86	3.78	1.32
	97	76.09	49.26	0.65	8.10	4.14	0.51	6.31	4.33	0.69	3.27	4.23	1.29
3S90	70	157.33	130.04	0.83	6.24	6.24	1.00	9.29	8.17	0.88	2.05	2.46	1.20
	73	151.79	124.07	0.82	6.33	6.27	0.99	9.13	7.97	0.87	2.09	2.53	1.21
	76	141.77	114.81	0.81	6.17	6.00	0.97	8.28	7.19	0.87	2.08	2.54	1.22
	79	135.07	107.92	0.80	6.23	5.89	0.95	8.00	6.88	0.86	2.13	2.62	1.23
	82	123.93	97.56	0.79	6.08	5.61	0.92	7.14	6.08	0.85	2.13	2.62	1.23
	85	116.17	89.72	0.77	6.17	5.44	0.88	6.82	5.72	0.84	2.20	2.74	1.25
	88	107.81	81.21	0.75	6.32	5.26	0.83	6.53	5.37	0.82	2.31	2.92	1.26
	91	98.96	72.42	0.73	6.50	5.01	0.77	6.24	5.00	0.80	2.46	3.16	1.28
	94	89.48	63.43	0.71	6.67	4.66	0.70	5.86	4.54	0.78	2.66	3.42	1.29
	97	79.43	54.32	0.68	6.90	4.24	0.61	5.48	4.05	0.74	2.93	3.76	1.28
3S95	70	173.02	149.92	0.87	5.29	5.29	1.00	8.53	7.74	0.91	1.92	2.18	1.13
	73	166.42	142.98	0.86	5.37	5.37	1.00	8.34	7.53	0.90	1.95	2.24	1.15
	76	159.18	135.72	0.85	5.37	5.37	1.00	7.99	7.18	0.90	1.97	2.27	1.15
	79	151.39	127.25	0.84	5.53	5.53	1.00	7.85	6.99	0.89	2.02	2.37	1.17
	82	142.94	118.45	0.83	5.61	5.61	1.00	7.55	6.66	0.88	2.09	2.45	1.17
	85	133.82	109.04	0.81	5.68	5.46	0.96	7.20	6.28	0.87	2.15	2.58	1.20
	88	124.05	98.82	0.80	5.84	5.30	0.91	6.92	5.93	0.86	2.26	2.73	1.21
	91	113.59	88.17	0.78	6.00	5.10	0.85	6.57	5.52	0.84	2.41	2.95	1.23
	94	102.45	77.21	0.75	6.16	4.77	0.78	6.16	5.04	0.82	2.58	3.23	1.25
	97	90.66	66.01	0.73	6.39	4.33	0.68	5.77	4.54	0.79	2.86	3.60	1.26

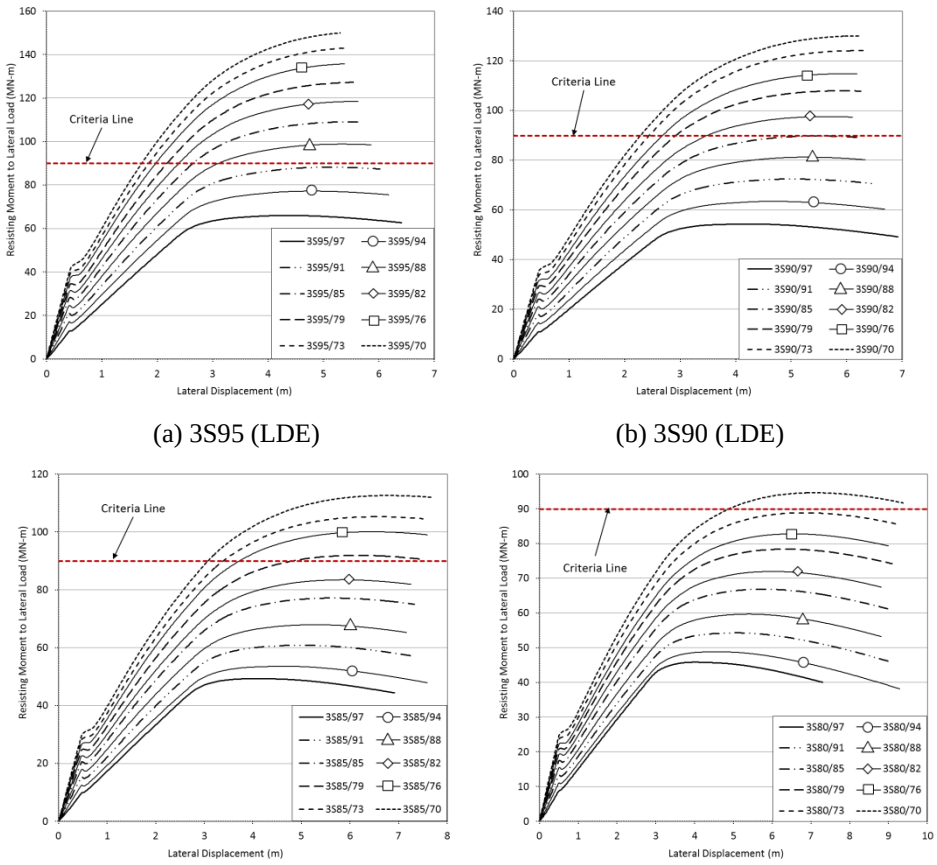

(a) 3S95 (LDE) (b) 3S90 (LDE)

(c) 3S85 (LDE) (d) 3S80 (LDE)

Fig. 14 Moment resisting capacity of designed DSCT towers for 3.6 MW turbines (LDE)

Fig. 16 shows the lateral load-lateral displacement relation of DSCT towers for 5.0 MW turbines with consideration of large displacement effect (LDE). In this case, the lateral load increases to the peak point and decreases after the peak point as displacement increase. When Fig. 16 is compared with Fig. 15, it is observed that the bending moment strengths decrease and by large displacement effect. Some design cases which were evaluated to be safe when large displacement effect was not considered such as 5S90/97, 5S85/94, and 5S80/83 are judged not to be safe. The bending moment resisting capacities in Fig. 16 are equal to the moment resisting lateral load (M_L) which is calculated by Eq. (16). The analysis results such as peak moment, dissipated energy, and energy ductility ratio of the designed DSCT towers for 5.0 MW turbines are summarized in Table 9.

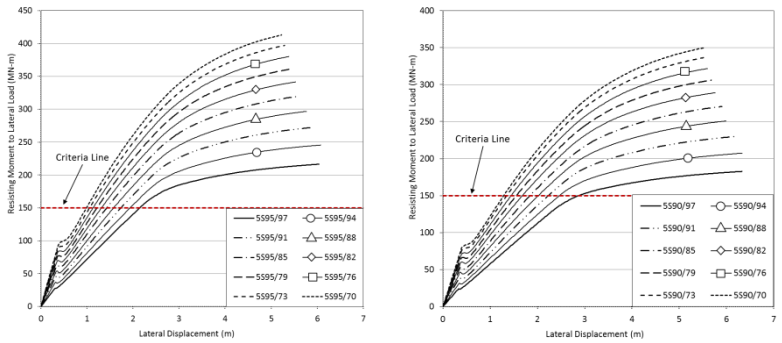

(a) 5S95 (SDE)

(b) 5S90 (SDE)

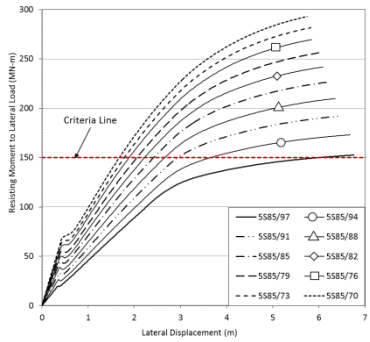

(c) 5S85 (SDE)

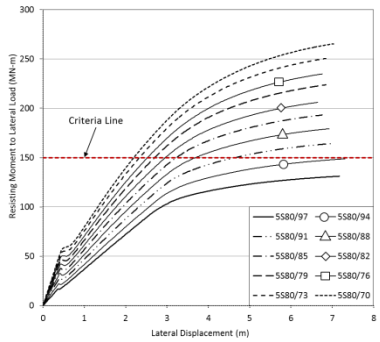

(d) 5S80 (SDE)

Fig. 15 Moment resisting capacity of designed DSCT towers for 5.0 MW (SDE)

In Figs. 13-16, the region, which the stiffness of a DSCT tower decreases and increases again after the end of linear region, is observed. The lateral load-displacement relation plot can be decomposed to the plots of component members, which are the concrete, the inner tube, and the outer tube as shown in Fig. 17. Fig. 17 shows that the stiffness reduction region after linear limit occurs in concrete. This stiffness reduction starts from loading step 3 as shown in Fig. 18(b) by the tensile failure of the concrete. After this region such as Figs. 18(c) and 18(d), the concrete resist much more bending moment as the compressive stress increases. Therefore, its stiffness starts to increase again.

As shown in Tables 8 and 9, a wind power tower could lose its bending moment capacity more than 30% by large displacement effect. The bending moment capacity reduction ratio by consideration of large displacement effect are plotted in Figs. 18(a) and 18(b) for the designed DSCT towers for 3.6 MW and 5.0 MW turbines, respectively. These plots show that a slender tower, which has a small diameter and a large hollow ratio, is much more sensitive to large displacement effect.

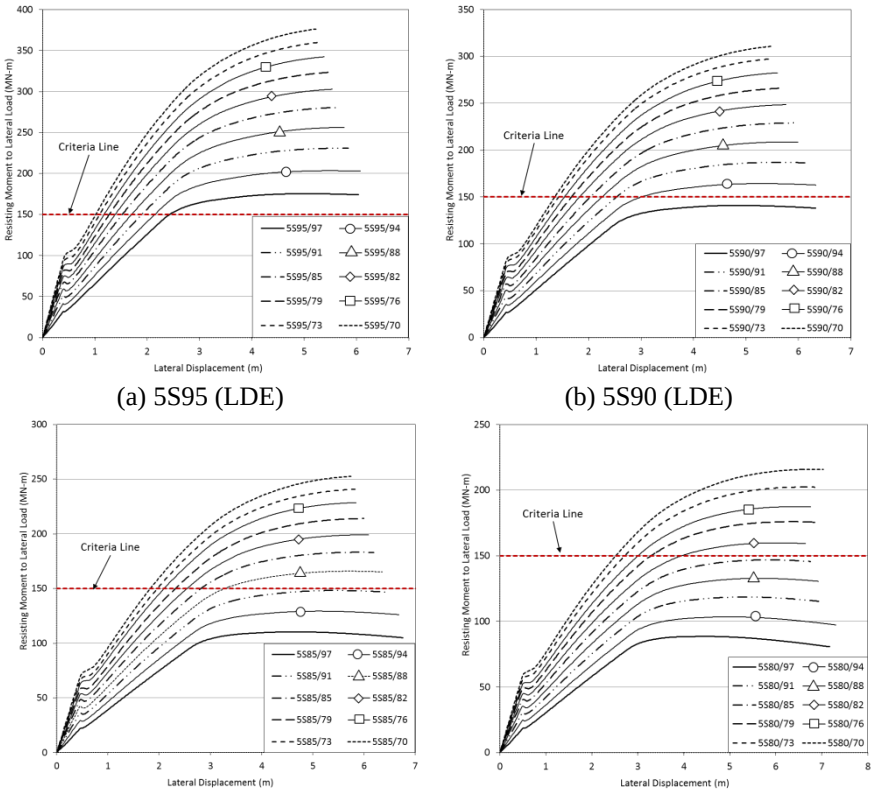

(a) 5S95 (LDE) (b) 5S90 (LDE)

(c) 5S85 (LDE) (d) 5S80 (LDE)

Fig. 16 Moment resisting capacity of designed DSCT towers for 5.0 MW turbines (LDE)

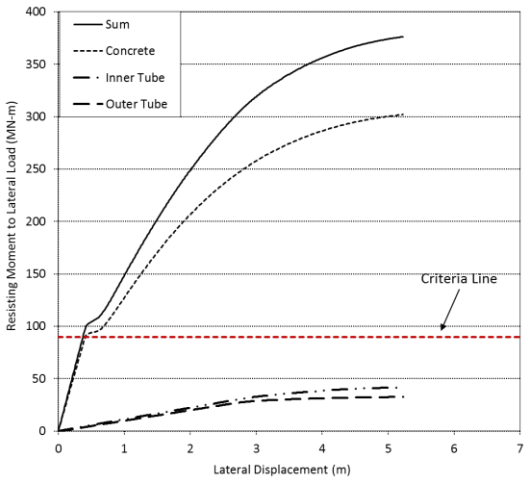

Fig. 17 Moment-displacement relation of each component member (5S95/70, LDE)

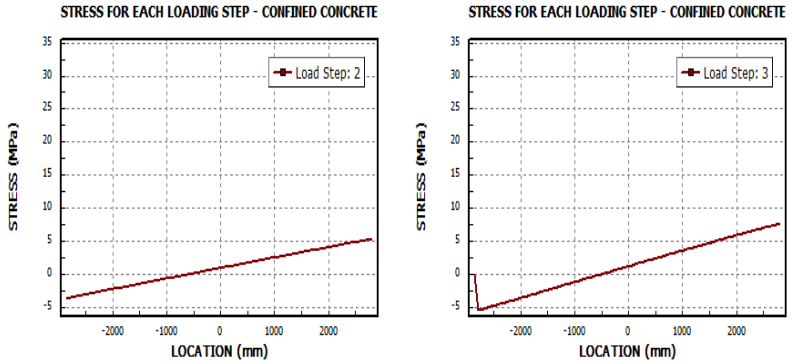

(a) Loading step = 2 (b) Loading step = 3

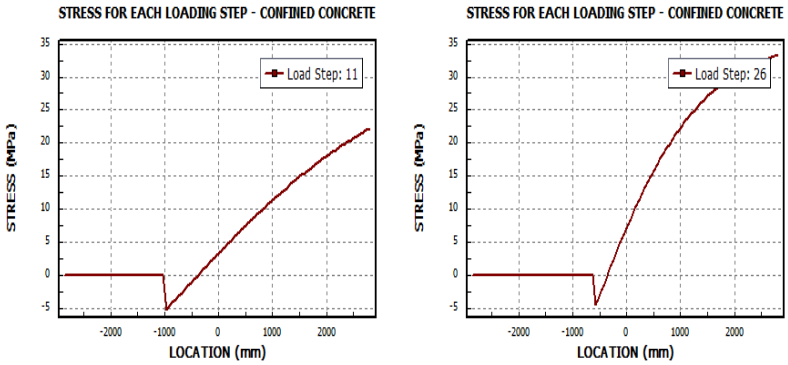

(c) Loading step = 11 (d) Loading step = 26

Fig. 18 Acting stress on concrete by loading step

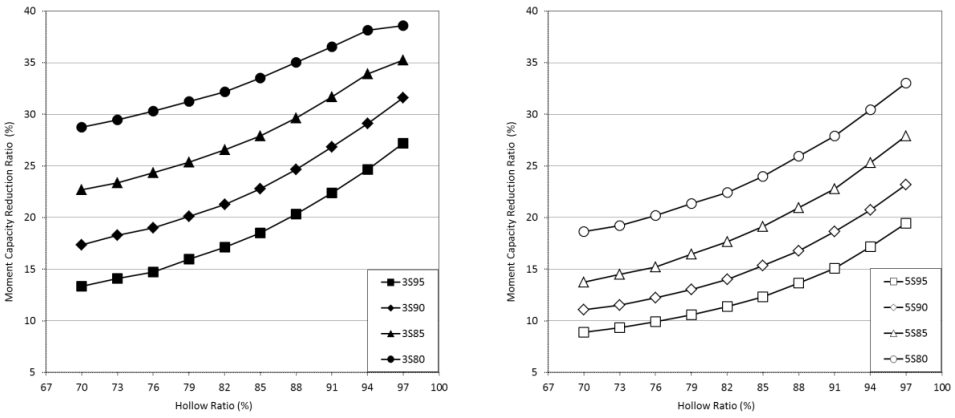

(a) DSCT tower for 3.6 MW turbine (b) DSCT tower for 5.0 MW turbine

Fig. 19 Moment resisting capacity reduction ratio by large displacement effect (M_W/M_n)

Table 9 Analysis result of DSCT wind tower for 5.0 MW turbine

Design case	Hollow ratio (%)	Peak moment (MN-m)			Displacement at peak moment (m)			Dissipated energy (MN-m)			Energy ductility ratio		
		SDE	LDE	LDE /SDE	SDE	LDE	LDE /SDE	SDE	LDE	LDE /SDE	SDE	LDE	LDE /SDE
5S80	70	257.23	215.87	0.84	7.31	6.86	0.94	16.16	13.53	0.84	2.12	2.54	1.20
	73	250.47	202.34	0.81	6.83	6.60	0.97	14.25	12.35	0.87	2.08	2.53	1.22
	76	234.77	187.39	0.80	6.74	6.43	0.96	13.15	11.31	0.86	2.07	2.56	1.23
	79	223.72	175.96	0.79	6.83	6.32	0.93	12.75	10.85	0.85	2.12	2.65	1.25
	82	205.97	159.81	0.78	6.63	6.01	0.91	11.35	9.57	0.84	2.11	2.66	1.26
	85	193.15	146.84	0.76	6.74	5.83	0.87	10.88	9.03	0.83	2.19	2.79	1.27
	88	179.25	118.59	0.66	6.90	5.31	0.77	10.42	7.76	0.74	2.30	3.15	1.37
	91	164.47	132.78	0.81	7.01	5.61	0.80	9.80	8.47	0.86	2.44	2.97	1.22
	94	148.74	103.46	0.70	7.28	4.95	0.68	9.35	7.13	0.76	2.65	3.46	1.30
	97	132.05	88.47	0.67	7.56	4.51	0.60	8.78	6.35	0.72	2.93	3.77	1.29
5S85	70	292.91	252.60	0.86	5.73	5.73	1.00	13.72	12.43	0.91	1.92	2.19	1.14
	73	281.69	240.79	0.85	5.81	5.81	1.00	13.42	12.08	0.90	1.94	2.23	1.15
	76	269.55	228.50	0.85	5.83	5.83	1.00	12.91	11.56	0.90	1.98	2.29	1.16
	79	256.18	214.06	0.84	5.98	5.98	1.00	12.63	11.21	0.89	2.02	2.36	1.17
	82	241.85	199.11	0.82	6.07	6.02	0.99	12.14	10.67	0.88	2.07	2.46	1.19
	85	226.47	183.16	0.81	6.17	5.86	0.95	11.63	10.09	0.87	2.15	2.58	1.20
	88	209.87	165.85	0.79	6.34	5.70	0.90	11.16	9.53	0.85	2.25	2.76	1.23
	91	191.98	148.21	0.77	6.41	5.42	0.85	10.39	8.70	0.84	2.38	2.93	1.23
	94	173.12	129.31	0.75	6.67	5.09	0.76	9.89	8.04	0.81	2.58	3.22	1.25
	97	153.15	110.39	0.72	6.94	4.64	0.67	9.29	7.25	0.78	2.85	3.61	1.27
5S90	70	349.61	310.91	0.89	5.50	5.50	1.00	15.77	14.59	0.92	1.94	2.14	1.11
	73	336.29	297.56	0.88	5.50	5.50	1.00	15.20	14.01	0.92	1.96	2.18	1.11
	76	321.70	282.42	0.88	5.58	5.58	1.00	14.79	13.56	0.92	1.99	2.23	1.12
	79	305.97	266.09	0.87	5.67	5.67	1.00	14.31	13.04	0.91	2.03	2.29	1.13
	82	288.93	248.46	0.86	5.75	5.75	1.00	13.76	12.45	0.90	2.08	2.39	1.15
	85	270.47	228.99	0.85	5.89	5.89	1.00	13.28	11.89	0.90	2.17	2.50	1.15
	88	250.73	208.70	0.83	5.97	5.82	0.97	12.56	11.12	0.89	2.26	2.65	1.18
	91	229.75	186.88	0.81	6.15	5.60	0.91	11.97	10.43	0.87	2.41	2.85	1.18
	94	207.27	164.25	0.79	6.31	5.28	0.84	11.22	9.57	0.85	2.58	3.14	1.21
	97	183.49	140.94	0.77	6.56	4.83	0.74	10.52	8.70	0.83	2.86	3.50	1.22
5S95	70	412.84	376.20	0.91	5.21	5.21	1.00	17.66	16.60	0.94	1.94	2.11	1.09
	73	396.97	359.91	0.91	5.28	5.28	1.00	17.20	16.12	0.94	1.97	2.14	1.09
	76	380.06	342.34	0.90	5.37	5.37	1.00	16.81	15.69	0.93	2.00	2.19	1.10
	79	361.57	323.30	0.89	5.44	5.44	1.00	16.27	15.11	0.93	2.04	2.25	1.10
	82	341.55	302.72	0.89	5.52	5.52	1.00	15.65	14.45	0.92	2.11	2.35	1.11
	85	319.94	280.55	0.88	5.60	5.60	1.00	14.94	13.69	0.92	2.18	2.43	1.11
	88	296.77	256.30	0.86	5.75	5.75	1.00	14.35	13.02	0.91	2.28	2.59	1.14
	91	271.91	230.86	0.85	5.83	5.74	0.98	13.43	12.05	0.90	2.41	2.77	1.15
	94	245.56	203.40	0.83	6.06	5.49	0.91	12.79	11.28	0.88	2.62	3.06	1.17
	97	217.61	175.34	0.81	6.29	5.04	0.80	12.00	10.33	0.86	2.90	3.48	1.20

5. Conclusions

A new-type structure, DSCT tower was tried to be adopted as a wind power tower. To know its feasibility of the application to a wind power tower, an automatic design tool was developed. Moreover, 80 sections of DSCT wind power towers designed by using the developed design tool. The automatically designed DSCT towers satisfied the required axial and bending strengths although they had smaller diameters. From this result, a DSCT column can be a possible candidate for the wind power tower in the future and the developed design program gives rational design sections.

For the designed DSCT wind towers, performance analyses were carried out with consideration of large displacement effect. Analysis results showed the designed sections were reasonable but large displacement effect makes the slender tower to lose much of its moment resisting capacity. Therefore, for the safety, large displacement effect should be considered in designing wind power towers.

Acknowledgments

This research was financially supported by the Ministry of Land, Infrastructure and Transport (MOLIT) of the Korea government (code 12 Technology Innovation E09) and Korea Institute of Ocean Science & Technology (project no. PE99323)

References

Chen, T.H. and Tran, V.T. (2015), "Prospects of wind energy on Penghu Island, Taiwan", *Wind Struct.*, **20**(1), 1-13.

Choi, E.H., Cho, J.R. and Lim, O.K. (2015), "Layout optimization for multi-platform offshore wind farm composed of spar-type floating wind turbines", *Wind Struct.*, **20**(6), 751-761.

Galleryhip, website: http://galleryhip.com

Han, T.H. (2014), *Auto DSCT manual Ver. 1.1*, Korea Institute of Ocean Science and Technology, Ansan, Korea.

Han, T.H. (2015), *CoWiTA manual Ver. 2.1*, Korea Institute of Ocean Science and Technology, Ansan, Korea.

Han, T.H., Stallings, J.M. and Kang, Y.J. (2010), "Nonlinear concrete model for double-skinned composite tubular columns", *Constr. Build. Mater.*, **4**(12), 2542-2553.

Han, T.H., Won, D.H., Kim, S. and Kang, Y.J. (2013), "Performance of a DSCT column under lateral loading: analysis", *Mag. Concrete Res.*, **65**(2), 121-135.

Khatri, D. (2013), *As Towers Grow Taller, Consider Structural Impacts*, North American Windpower, **10**(7), 7-11.

Kilpatrick A.E. and Ranagan B.V. (1997), *Deformation-control analysis of composite concrete columns*, Research Report No. 3/97, School of Civil Engineering, Curtin University of Technology, Perth, Western Australia.

Korea Concrete Institute (2012), *Concrete Structure Design Code*, Seoul.

Ljjj L.B.J. and Gravesen, H. (2008), *Kriegers Flak Offshore Wind Farm - Design Basis Foundations*, Vattenfall Vindkraft AB.

Ruralgrubby's Wind Watch, website: http://ruralgrubby.wordpress.com

Sawyer, S. (2013), "Global wind power overview", *Wind Energy Asia*, 76-90.

Shakir-Khalil, H. and Illouli, S, (1987), "Composite columns of concentric steel tubes", *Proceedings of the Conference on the Design and Construction of Non-Conventional Structures*.

Sung, J.K. (2012), "Current Status of Wind Power Industry and Offshore Wind Projects", *Korea-Europe Wind Plaza 2012.*

Tao, Z., Han, L.H. and Zhao, X.L. (2004), "Behavior of concrete-filled double skin (CHS inner and CHS outer) steel tubular stub columns and beam columns", *J. Constr. Steel Res.*, **60**, 1129-1158.

Teng, J.G., Yu, T., Wong, Y.L. and Dong, S.L. (2006), "Hybrid FRP-concrete-steel tubular columns: concept and behavior", *Constr. Build. Mater.*, **21**, 846-854.

Timoshenko, S.P. and Gere, J.M. (1963), *Theory of Elastic Stability*, 2nd Ed., McGraw-Hill, Singapore

Unchai, T. and Janyalertadun, A. (2014), "CFD Evaluation of a suitable site for a wind turbine on a trapezoid shaped hill", *Wind Struct.*, **19**(1), 75-88.

Wei, S., Mau, S.T., Vipulanandan, C. and Mantrala, S.K. (1995), "Performance of new sandwich tube under axial loading: Experiment", *J. Struct. Eng. - ASCE*, **121**, 1806-1814.

Wei, S., Mau, S.T., Vipulanandan, C. and Mantrala, S.K. (1995), "Performance of new sandwich tube under axial loading: Analysis", *J. Struct. Eng. - ASCE*, **121**, 1815-1821.

Yu, T., Wong, Y.L., Teng, J.G., Dong, S.L. and Lam, E.S.S. (2006), "Flexural behavior of hybrid FRP-concrete-steel double-skin tubular members", *J. Compos. Constr. - ASCE*, **10**(5), 443-452.

Zhao, X.L. and Grzebieta, R. (2002), "Strength and ductility of concrete filled double skin (SHS inner and SHS outer) tubes", *Thin. Wall. Struct.*, **40**, 199-213.

Nomenclature

$A_{i,j}^{CC}$ cross sectional area of the j th element of concrete at the i th stage of strain distribution
$A_{i,j}^{IT}$ cross sectional area of the j th element of inner tube at the i th stage of strain distribution
$A_{i,j}^{OT}$ cross sectional area of the j th element of outer tube at the i th stage of strain distribution
C_b distance from neutral axis to near outer surface
D outer diameter of confined concrete
D_i diameter of hollow section or inner diameter of confined concrete
E modulus of elasticity of outer tube
E_i modulus of elasticity of inner tube
F_{eq} equivalent fatigue lateral load
F_{ex} extreme lateral load
F_{op} operational lateral load
f_c stress acting on concrete
f_{cr} buckling strength of outer tube
f_{iy} yield strength of the inner tube
f_s stress acting on steel
f_y yield strength of outer tube
$f_{i,j}^{CC}$ stress acting on the j th element of concrete at the i th stage of strain distribution
$f_{i,j}^{IT}$ stress acting on the j th element of inner tube at the i th stage of strain distribution
$f_{i,j}^{OT}$ stress acting on the j th element of outer tube at the i th stage of strain distribution
h height of tower or column
h_T height from top of footing to center of hub
L_p length of plastic hinge
M_{eq} equivalent fatigue moment
M_{ex} extreme moment
M_i moment at the i th stage of strain distribution
M_i^{CC} moment acting on concrete at the i th stage of strain distribution
$M_{i,j}^{CC}$ moment acting on the j th concrete element at the i th stage of strain distribution
$M_{i,j}^{IT}$ moment acting on the j th inner tube element at the i th stage of strain distribution
$M_{i,j}^{OT}$ moment acting on the j th outer tube element at the i th stage of strain distribution

M_i^{IT} moment acting on inner tube at the i th stage of strain distribution

M_i^{OT} moment acting on outer tube at the i th stage of strain distribution

M_{op} operational moment

M_L resisting moment to lateral load

M_n nominal bending strength or moment resisting capacity

M_W moment induced by weight of turbine

$M(z)$ moment function

P_i axial load at the i th stage of strain distribution

P_i^{CC} axial load acting on core concrete at the i th stage of strain distribution

P_i^{IT} axial load acting on inner tube at the i th stage of strain distribution

P_i^{OT} axial load acting on outer tube at the i th stage of strain distribution

$P_{i,j}^{CC}$ axial load acting on the j th concrete element at the i th stage of strain distribution

$P_{i,j}^{IT}$ axial load acting on the j th inner tube element at the i th stage of strain distribution

$P_{i,j}^{OT}$ axial load acting on the j th outer tube element at the i th stage of strain distribution

P_L lateral load or wind load

$S_{i,j}$ length of the j th column element at the i th stage of strain distribution

t thickness of outer tube

t_i thickness of inner tube

W_N turbine weight

$x_{i,j}^{CC}$ distance from neutral axis to center of j th concrete element at the i th stage of strain distribution

$x_{i,j}^{IT}$ distance from neutral axis to center of j th inner tube element at the i th stage of strain distribution

$x_{i,j}^{OT}$ distance from neutral axis to center of j th outer tube element at the i th stage of strain distribution

Δ_i lateral displacement of column at the i th stage of strain distribution

$\Delta_{i,j}$ lateral displacement of the j th column element at the i th stage of strain distribution

Δ_N lateral displacement of center of gravity of turbine.

ε axial strain of concrete

ν Poisson's ratio of outer tube

φ_i curvature of column at the i th stage of strain distribution

$\varphi(z)$ curvature function

$\theta_{i,j}$ rotation angle of the j th column element at the i th stage of strain distribution